

GALAXY POPULATIONS AND EVOLUTION IN CLUSTERS II: DEFINING CLUSTER POPULATIONS

CHRISTOPHER J. CONSELICE^{1,2,3}, JOHN S. GALLAGHER, III³, ROSEMARY F.G. WYSE^{4,5}

Accepted to the Astronomical Journal

ABSTRACT

This paper presents quantitative techniques for studying, in an unbiased manner, the photometric and structural properties of galaxies in clusters, including a means to identify likely background objects in the absence of redshift information. We develop self-consistent and reproducible measurements of fundamental properties of galaxies such as radius, surface brightness, concentration of light and structural asymmetry. We illustrate our techniques through an application to deep UBR images, taken with the WIYN 3.5m telescope, of the central ~ 173 arcmin² (or $0.3 \text{ Mpc} \times 0.3 \text{ Mpc}$) of the cluster Abell 0146 (Perseus). Our techniques allow us to study the properties of the galaxy population in the center of Perseus down to $M_B = -11$. Using these methods, we describe and characterize a well-defined relation between absolute magnitude and surface brightness for galaxy cluster members across the entire wide range of galaxy luminosity from $M_B = -20$ to $M_B = -11$ independent of galaxy type. The galaxies that are assigned by our techniques to the background show no such tight relationship between apparent magnitude and surface brightness, with the exception of those we identify as being members of a background cluster of galaxies at $z \sim 0.55$. We, however, find that at the fainter magnitudes, $M_B > -16$, there is a large scatter about the underlying color-magnitude relation defined by the brighter galaxies. Our analysis of galaxies at the center of the Perseus cluster further indicates that the vast majority are ‘normal’, with little evidence for structural or photometric properties associated with active evolution; we however discuss the detailed properties of a handful of unusual galaxies. Finally, the galaxy luminosity function of the Perseus cluster center is computed, with a derived faint end slope of $\alpha = -1.44 \pm 0.04$, a value similar to those previously obtained for other nearby rich galaxy clusters.

Subject headings: galaxies: evolution — galaxies: structure — galaxies: fundamental parameters (classification, colors, radii, luminosities) — galaxies: clusters: individual (Perseus) — galaxies: dwarf — galaxies: elliptical and lenticular

1. INTRODUCTION

The oldest (mean ages > 10 Gyr) and most apparently quiescent galaxies, without obvious evidence for recent star-formation or interactions with other galaxies, in the local Universe are giant ellipticals found in rich clusters of galaxies. These rich clusters contain a wide range of galaxy types, including a large population of low-mass systems (Ferguson & Binggeli 1994), whose history may well be very different from that of the giant ellipticals (Conselice, Gallagher & Wyse 2001a; hereafter Paper I, and references therein). Investigations across the range of galaxy populations in an individual cluster can provide insight into the past evolution of galaxies in these extreme environments, and can constrain on-going processes. Both bright and faint galaxies in the nearby Coma and Virgo clusters are now well studied and characterized (e.g., Binggeli, Sandage & Tammann 1985; Thompson & Gregory 1993; Secker, Harris & Plummer 1997; Vazdekis et al. 2001; Paper I) revealing basic photometric and spectroscopic properties of these systems. However, the nearby Bautz-Morgan class II-III cluster Perseus (Abell 462) with a redshift $V_r = 5366 \text{ km s}^{-1}$ (Struble & Rood 1999) and

distance⁶, $D = 77 \text{ Mpc}$, has not yet been studied in detail, partly due to its low Galactic latitude ($b \sim -13^\circ$). This paper is a first step towards such a study.

In addition to being one of the nearest rich clusters, Perseus is exceptional in several ways. It is the brightest observed X-ray cluster (e.g. Nulsen & Fabian et al. 1980; Ulmer et al. 1980) with possibly a large cooling flow centered on the extraordinary galaxy NGC 1275 (e.g. Allen & Fabian 1997). The Perseus cluster also has one of the highest known internal cluster velocity dispersions, $\sigma = 1260 \text{ km s}^{-1}$ (Kent & Sargent 1983), and a strong morphological segregation, with few spiral galaxies found in its densest regions (e.g., Brunzendorf & Meusinger 1999). The peculiar central galaxy, NGC 1275 (Perseus A), is a strong radio source, has a non-thermal active nucleus and unusual stellar components, as well as a spectacular system of optical emission line filaments (e.g., Conselice, Gallagher & Wyse 2001b, and references therein). As argued in Conselice et al. (2001b), a recent merger/accretion of a small group of galaxies into the cluster may be responsible for several of these manifestations.

The Perseus cluster, as revealed through galaxy counts,

¹ California Institute of Technology, Mail Code 105-24, Pasadena, CA

² Space Telescope Science Institute, 3700 San Martin Drive, Baltimore, MD

³ Department of Astronomy, University of Wisconsin, Madison 475 N. Charter St. Madison, WI

⁴ School of Physics & Astronomy, University of St. Andrews, Scotland

⁴ Permanent address: Department of Physics & Astronomy, The Johns Hopkins University

⁶ Using $H_0 = 70 \text{ km s}^{-1} \text{ Mpc}^{-1}$

has a compact core, with a size 0.1 Mpc, and a unimodal structure, as opposed to the double structure found in, for example, the Coma cluster (e.g., Colless & Dunn 1996). There is no significant spatial clumping in the distribution of brighter cluster galaxies, although the nearly linear array of galaxies near its center may signify the presence of weak substructure. The galaxies in the Perseus cluster also have a smooth gaussian-like velocity distribution (Girardi et al. 1997), although both Slezak, Durret, & Gerbal (1994) and Mohr, Fabricant, & Geller (1993) find some evidence of substructure in the X-ray emission. Perseus also harbors an exceptionally large population of radio head-tail sources, including NGC 1275 (Sijbring & DeBruyn 1998). These sources are possibly the result of interactions between the host galaxies and the intracluster medium, with the large cluster velocity dispersion resulting in stronger ram pressure forces ($\propto v^2$) compared to a more typical cluster with slower relative velocities between galaxies and the ICM. These extreme conditions make the core region of Perseus unique in the nearby universe and could have a strong effect on the state and evolution of its galaxies. However, the same basic physical mechanisms should be occurring in all clusters and they are perhaps faster or stronger in Perseus, making evolutionary effects easier to study.

However, as the Perseus cluster is one of the richest systems in the nearby universe, and is at a distance significantly less than that of the Coma cluster (Baum et al. 1997), it represents a good opportunity to study the signatures of dynamical and photometric evolution of galaxies in such environments, including the intrinsically faint members. The development of the necessary tools for such a program is the aim of the present paper, while a companion paper (Conselice et al. 2002; hereafter Paper III) presents details of the results of an investigation of faint Perseus cluster members.

In this paper we define global photometric and structural parameters for galaxies, taking care to adopt measuring techniques which will be useful for comparisons between galaxy clusters. For example, commonly used isophotal magnitudes are ill-suited for comparing galaxies observed in different conditions, and especially at different distances where the ratio of metric to isophotal radii can vary strongly. As a result, the use of isophotal radii can bias studies of both galaxy evolution and cosmology (Petrosian 1976; Sandage & Perelmuter 1990; Dalcanton 1998). We therefore adopted Petrosian radii to measure sizes of galaxies and to define photometric apertures.

Additionally, it has become clear recently that structural parameters can reveal much about the evolutionary state of galaxies (e.g., Abraham et al. 1994; Conselice 1997; Conselice, Bershady & Jangren 2000; Bershady, Jangren & Conselice 2000). Attempts have also been made for some time to classify individual galaxies in clusters using structural parameters (e.g., Ichikawa, Wakamatsu & Okamura 1986), although no systematic classification system has yet been presented. This paper presents the framework of such a system in clusters (see §4.3). We developed techniques to distinguish between cluster and background galaxies, as well as methods for quantifying galaxy structures using the asymmetry and concentration indexes. In galaxies there are essentially two ‘ages’ related to the star-formation his-

tory and to the mass assembly history respectively, and photometry helps decipher the former, and structure the latter.

Photometry of bright cluster galaxies has revealed the existence of a well-defined correlation between the color and magnitude of elliptical galaxies (e.g., Kormendy 1977; Bower, Lucey & Ellis 1992), such that fainter galaxies are bluer. This is normally interpreted as a metallicity effect, with redder ellipticals being more metal-rich (e.g. Larson 1974; Kauffmann & Charlot 1998; Vazdekis et al. 2001). The data we present here allow us to investigate such scaling relations, and others between the photometric and structural parameters down to very faint intrinsic luminosities, $M_B \sim -11$. These faint low-mass galaxies appear to be dwarf ellipticals; we however denote these galaxies using the more general term ‘low-mass cluster galaxy (LMCG)’ (a nomenclature we adopt also in Paper III), so as to not bias the interpretations of what these objects are. We also compare observed UBR color-color diagrams with the predictions for old stellar populations with a range of metallicities, and find results that support the interpretation that the range of colors of ellipticals in Perseus can be explained by metallicity differences (see Paper III for a full analysis).

This paper is organized as follows: in §2 we describe the data and analysis techniques, §3 is a discussion of background galaxy contamination, §4 describes an analysis of the data set, and §5 contains a summary. We assumed a distance to the Perseus cluster of 77 Mpc throughout this paper, giving a scale of ~ 20 kpc per arcmin.

2. OBSERVATIONS AND REDUCTIONS

All of the imaging data used in this paper, and in Paper III, were taken with the WIYN 3.5m f/6.2 telescope located on Kitt Peak. The B and R images were acquired with a thinned 2048² pixel S2kB charged coupled device (CCD). The scale for these images is 0.2'' pixel⁻¹, with a field of view 6.8' \times 6.8'. The imaging took place on the nights of 1998 November 14 and 15, under photometric conditions. The average seeing for all images was 0.7''. The images of the Perseus cluster were taken in four different fields towards the center of the cluster. Harris B and R, as well as narrow band H α , filters were used on each of the four fields. The exposure times were 2400 sec in R, and 2000 sec in B. The H α images were discussed in Conselice et al. (2001b). Figure 1 shows a mosaic image of the area covered in this paper and in Paper III.

Ten flat fields were obtained in each filter prior to each night of observing with the S2kB. A single flat field for each filter for each night was created by taking the median of its respective flats. A constant zero level pedestal was determined from the over-scan region, and subtracted, rather than using standard bias frames, since it was discovered that adopting the latter technique increases the uncertainty in photometry obtained from this CCD.

To perform accurate photometry on the galaxies in these fields, we align and transform the B images to match the R images. A simple linear interpolation was found to be inadequate, as the point spread function (PSF) for each filter varied differently with position on the CCD, and small scale differences also exist. We therefore used a non-linear 2nd order fitting routine to match the positions of

objects, including corrections for slight rotations between the B and R frames. As a result, the B and R frames are matched to within an rms of 0.2 pixels, or 0.04''.

We also obtained UBR-band images with the WIYN Mini-Mosaic camera for two $9.6' \times 9.6'$ fields around the center of the four combined S2kB fields. Mini-Mosaic consists of two SITe 4096×2048 CCDs separated by a gap of 5'' and with a scale of $0.14'' \text{ pixel}^{-1}$. Exposure times for the U band images are 2400 sec per field, resulting in good photometry for the cluster galaxies, with shorter exposure Harris B and R images taken for calibration purposes only. The images were reduced using the IRAF package MSC, with flat fielding and alignment done in the same manner as for the S2kB images, but with the bias subtraction performed in the standard manner using bias frames. During the Mini-Mosaic imaging run the seeing in the U band images was 0.9''.

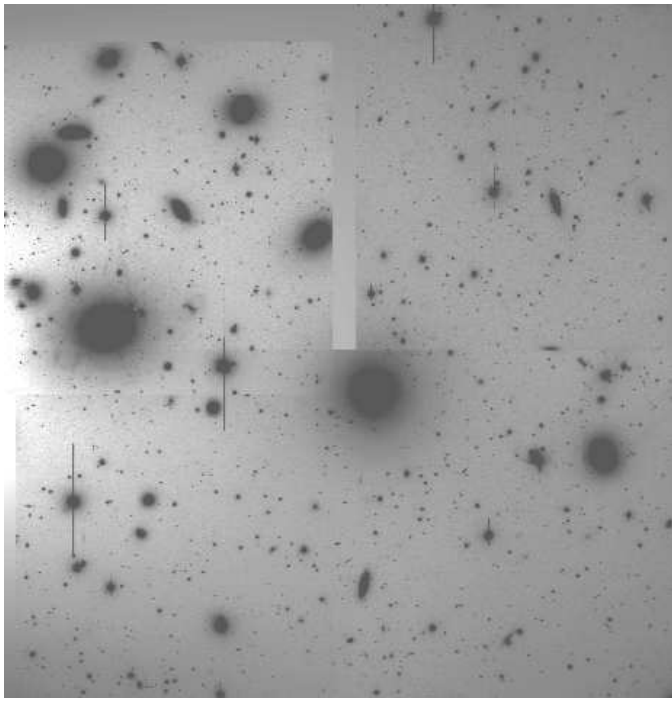


FIG. 1.— Mosaic image of the central 173 arcmin^2 of the Perseus cluster imaged by WIYN in the R band and studied in this paper. NGC 1275 is the large galaxy in the left (east) part of the image.

2.1. Photometry

Images of Landolt standard star fields were taken throughout each night, and as a result, we are able to fit accurate zero points, airmasses, and color terms, for both nights. We fit the following photometric solution for each of the B-band and R-band S2kB data:

$$F_{B,R} = f_{B,R} + a_1 + a_2 \times X_{B,R} + a_3 \times (B - R), \quad (1)$$

where $F_{B,R}$ is the magnitude of an object, $f_{B,R}$ is the instrumental magnitude, X is the airmass of the observation, while a_1, a_2, a_3 are the zero point offset, airmass and color terms. Higher order color terms were also allowed initially, but were found to be smaller than the photometric random errors, and so were left out of the final photometric calibration. The coefficients a_i were set to be constant throughout each night. The standard star calibration provides

magnitudes with RMS random errors of $\Delta \text{mag} \sim 0.04$ in B and $\Delta \text{mag} \sim 0.03$ in the R band. To correct for Galactic extinction, we first investigated the amplitude of any variation over the area studied here through examination of the COBE/DIRBE and IRAS/ISSA maps from Schlegel, Finkbeiner & Davis (1998). These maps show that Galactic absorption in the B-band varies by only 0.03 mag over $15'$. Most of this variation is due to one small area of lower than average extinction. These variations are equal to, or lower than, the random photometry errors and are hence ignorable. For the correction, we adopted the value of $E(B-V) = 0.171$ and $R_V = 3.1$ and the empirical relations of Cardelli, Clayton and Mathis (1989). We also correct for the slight k-correction, using the prescriptions of Poggianti (1997).

The Mini-Mosaic data, taken 13 months later, were calibrated in the same manner. There is considerable overlap between the Mini-Mosaic and S2kB fields and thus we can make a direct comparison to determine the accuracy of the photometric calibration as a function of magnitude. Figure 2 shows the result of such a comparison between the B magnitudes and $(B-R)$ colors for the galaxies in the overlapping regions of the two fields-of-view – the photometry, carried out on two completely different detectors, over a year apart, and with different standard star calibrations, is stable and robust. The scatter of the difference is low for the brightest galaxies, $\text{RMS} \sim 0.05$ mag, while the fainter galaxies have a larger scatter. Often the most deviant points are due to residual stellar light contamination in the aperture used (see §2.2 below for a discussion of our techniques to remove stars).

2.2. Galaxy Detection and Star Removal

We detected both galaxies and stars with the FOCAS software package (Jarvis & Tyson 1981). A detection threshold of 5σ above the sky is used to find only modestly faint galaxies and not the vast number of faint, low surface brightness galaxies, which are probably mostly background objects. We furthermore used a strict deblending criterion to remove detections of globular clusters often seen near many of the giant galaxies. The deblending parameters adopted are appropriate for the case at hand, in which most of the objects are early-type galaxies without significant substructure, and the routine does not split single galaxies into several spurious separate detections. FOCAS does not detect the brightest galaxies, thus these are added in by hand, as are any obvious galaxies that FOCAS misclassified as stars due to their bright nuclei. After removing objects classified by FOCAS as stellar, and adding in the brighter galaxies, our final catalog contains 904 galaxies over the 173 arcmin^2 of the survey. As we argue below, most of these objects are background galaxies.

Photometry of galaxies in the Perseus cluster is complicated by its low Galactic latitude, and the resulting presence of numerous foreground Galactic stars. We subtracted the occasional overlapping stellar images prior to obtaining photometry for the galaxies using the point-spread function fitting and subtraction routines in the IRAF DAOPHOT package. The stellar PSF was characterized as a function of magnitude empirically, from measurements of stellar images of different magnitudes spread across the field. It proved possible to remove all the light

from most stars to within 1%. We then used these star-subtracted images for all further analysis of the photometry and structural parameters of Perseus galaxies.

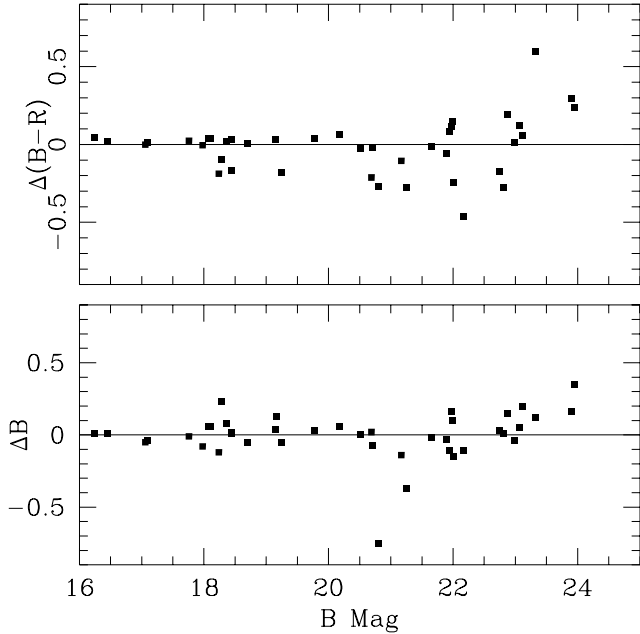


FIG. 2.— Difference in measured (B–R) color and apparent B magnitudes for galaxies observed with both the Mini-Mosaic and S2kB CCD cameras on the WIYN telescope. The Mini-Mosaic data are not as deep in the B and R bands as they are in the S2kB images.

2.3. Different Measurements of Radius

Defining a galaxy's radius is not trivial, and many methods exist, including the traditional and popular approach of measuring a radius out to an isophotal level, such as the $\mu_{pg} = 26.5$ mag arcsec $^{-2}$ Holmberg radius. While almost any consistently measured 'radius' would be adequate for this study, it would be inaccurate, and perhaps irresponsible, to use radii that are not reproducible in other clusters and galaxies at various distances, something which isophotal radii are ill-suited to do. Even so-called metric radii that are based on the percentage of light within an aperture are often based on "total" light measurements that are isophotally biased.

To overcome these difficulties, we use the inverted form of the Petrosian radius (Petrosian 1976; Kron 1995). The inverted Petrosian parameter, η , is the ratio of the local surface brightness $l(\theta)$ at a given angular distance, θ , from the center of the galaxy to the mean surface brightness within θ , assuming circular apertures and azimuthal averaging:

$$\eta = \frac{1}{2} \frac{d\ln l(\theta)}{d\ln \theta} = \frac{I_\theta}{\langle I \rangle_\theta}. \quad (2)$$

The inverted Petrosian radius parameter is defined as the projected radius at which η equals some value between 1 and 0. In general, the lower the value of η the larger the value of the Petrosian radius. The Petrosian radii were found by Bershady et al. (2000) and Conselice et al. (2000a) to be the most consistent and robust measures of radius to use in the derivation of structural parameters of galaxies and have been used for cosmological and galaxy

evolution work (e.g., Sandage & Perelmutter 1990; Sandage & Lubin 2001; Blanton et al. 2001).

We used the $R_p = 3 \times r(\eta = 0.5)$ radius to measure the total light in a galaxy from which half-light radii, 'total' magnitudes and colors are derived. The R_p radius defined in this way has values similar to the $\eta = 0.2$ radius where $\sim 99\%$ of the light of most galaxies is contained (Bershady et al. 2000). We chose the present definition since for faint galaxies, which are often barely resolved, as in our case, the derivation of the $\eta = 0.2$ radius often never converges, and experimentation revealed that $\eta = 0.5$ was the most reliable physical radius that corresponded well to subjective eye estimates of galaxy sizes. Further experimentation with a high redshift cluster, MS-1054, confirms the reliability of R_p for measuring metric radii (Conselice et al. 2002 in preparation).

2.4. Photometric Errors and Completeness

This paper includes photometry of faint galaxies which have magnitudes $m_B < 25$ within R_p . Each galaxy has an associated random error based on its individual photometric measurement within R_p . We performed limited Monte-Carlo simulations to determine how accurate these estimated random errors are, and to search for any systematic errors that may be present across our images.

To do this we created 20 simulated galaxies, multiple times, all at the same magnitude and place them randomly in the Perseus fields. These simulated galaxies range in magnitude in B and R from 18.5 to 24.5, all with exponential profiles that match dwarf galaxies, and half-light radius (equal to 1.7 exponential scale-lengths) similar to a typical Perseus low mass cluster galaxy with a half-light radius of 2''. This size also ensures that the surface brightness of the simulated objects is similar to that of the faintest objects in our study. Each galaxy in the simulations has its magnitude measured following the same techniques and methods used to compute magnitudes of actual Perseus galaxies, as outlined above.

Figure 3 shows the results of these simulations for retrieved magnitudes and colors. The triangles in Figure 3a show the average difference between measured and input magnitudes as a function of input magnitude in the B-band image, while boxes represent the average differences in the R-band image. The error bars in Figure 3 represent the 1σ variation of the differences. Figure 3b shows the average retrieved color differences and their 1σ variations. These simulations show that it is possible to measure very reliably the magnitudes and colors of objects down to an absolute magnitude $M_B \sim -12.5$ at the assumed distance and with reddening accounted for. At $M \sim -12.5$ the mean uncertainties are: $\langle (R_{\text{sim}} - R_{\text{meas}}) \rangle = 0.04 \pm 0.03$, $\langle (B_{\text{sim}} - B_{\text{meas}}) \rangle = 0.03 \pm 0.01$ and $\langle (B - R)_{\text{sim}} - (B - R)_{\text{meas}} \rangle = -0.02 \pm 0.03$. These are similar to or less than the observational errors at our magnitude limit. There are therefore no strong systematic errors in measurements down to $M = -12.5$, and the reported photometric random errors are likely accurate. We can reach somewhat fainter limits but with an increased systematic uncertainty.

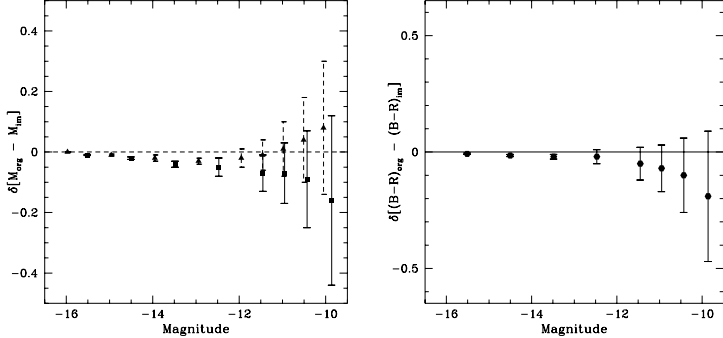


FIG. 3.— Results of Monte Carlo simulations performed by placing simulated galaxies in the images used in this paper. The left panel shows the resulting magnitude difference between the original and input magnitude, M_{im} as a function of the input magnitude, converted into absolute values assuming these objects are at the distance of the Perseus cluster. The squares represent the simulations done in the R band, while the triangles are for the B band. The error bars are formal 1σ variations of the average differences. The right panel shows the difference between the input and output colors. These results support the validity of our data reduction procedures for objects down to $M_B = -11$.

Figure 4 is a plot of the number counts for all galaxies detected by FOCAS in the sample area (173 arcmin^2). The number counts turn over fainter than $m_B = 23.5$, and as such they are not complete to magnitudes fainter than this. This corresponds to $M_B = -10.7$, about a magnitude fainter than the limit reached by previous studies of the Perseus cluster luminosity function (De Propris & Pritchett 1998). It is possible that we are not complete at brighter magnitudes if the true counts are steeper than we observe. All results pertaining to complete samples, such as luminosity functions, will be examined at magnitudes brighter than this limit, i.e., $M_B < -11$.

2.5. Structural Parameter Definitions

We performed photometry on each of the 904 galaxies in our sample using the APHOT package in IRAF. APHOT is an aperture photometry program that allows users to choose various photometric apertures, as well as centering and sky fitting routines. For each galaxy, we fit the sky using an annulus of width 10 pixels, and radius 100 pixels ($20''$), centered on the galaxy. While we tried smaller annuli and generally produced the same results, we favored the larger annulus radius as our images were generally flat and the larger number of pixels allows a better estimate of the true background and reduced the significance of any contamination from other galaxies as more sky area is covered. We adopted the centroid of each galaxy's light distribution as the center for the photometry routines. Total magnitudes and colors within the R_p radius were measured from the UBR frames. We also measured the central surface-brightness μ_B , defined as the mean surface brightness within the central $2''$ of each galaxy. A central color is also measured within the same radius.

We also computed for each galaxy the half-light or effective radius, R_e , defined as the point on the curve of growth where half of a galaxy's light (based on the total magnitude out to the Petrosian radius we adopt) is contained. Another photometric parameter we compute is the concentration index, C , defined as the ratio of the radii containing 80% (r_{80}) and 20% (r_{20}) of a galaxy's light

(e.g., Kent 1985; Bershady et al. 2000),

$$C = 5 \times \log \left(\frac{r_{80}}{r_{20}} \right). \quad (3)$$

A higher value of C implies that the light in that galaxy is more concentrated towards the center, and likewise, a lower C value indicates the light is less concentrated. Typically early-type galaxies have the highest C value, while later types have lower values (Bershady et al. 2000). Within the R_p radius a simulated galaxy with an $r^{1/4}$ surface brightness profile has a concentration value $C = 3.2$, while a pure exponential disk has $C = 2.5$, and a constant surface brightness system has $C = 1.5$.

The other quantitative morphological parameter we use is the asymmetry index A (Conselice 1997, Conselice et al. 2000a), a parameter that measures the deviation of a galaxy's light from perfect 180° symmetry. Mathematically, it is defined as

$$A = \min \left[\frac{\Sigma |(I_o - I_{180})|}{\Sigma |I_o|} \right] - \min \left[\frac{\Sigma |(B_o - B_{180})|}{\Sigma |B_o|} \right], \quad (4)$$

where I represents the intensity values of the image pixels, the subscript indicating the rotation angle, and B represents a blank region containing background light. The second term is used to correct for sky and noise effects. The more disturbed the structure of a galaxy is, the higher the measured asymmetry, A (§4.3.1).

2.6. Morphological Classifications

One of the key tools for understanding galaxies is to classify them into distinct populations (e.g., van den Bergh 1998). This is especially true for the members of galaxy clusters (see Paper I for a longer discussion). Although ideally we would classify galaxies without the use of subjective eyeball classifications, it is still necessary to do this at some level to calibrate the more objective, automatic classification techniques and to place galaxies in rough population classes.

We classified galaxies in these images by carefully examining each object, and placing them into 6 rough morphological types. These are: giant ellipticals, low-mass cluster galaxies (LMCGs), early-type spirals, late-type spirals, peculiar galaxies and background galaxies. Lenticular (S0) galaxies were placed into the early-type spiral galaxy bin.

Giant ellipticals are defined in this paper as large, high surface brightness, mostly symmetric, objects without the presence of an outer disk. Ellipticals also have high concentration values and low asymmetries (Conselice et al. 2000a). Early and late-type spirals are objects with disks and/or spiral patterns. Early-type disks are galaxies whose bulges are roughly brighter than their disks, or with an estimated $B/D > 1$, while late-type disks are those where the disk light dominates the bulge, or an estimated $B/D < 1$. Peculiar galaxies are ones that do not fit into the classical Hubble sequence. In our Perseus cluster sample, this category includes one possible merger, and one interesting galaxy near NGC 1275 that is symmetric, but with an unusual structure (see §4.5 and Conselice, Gallagher & Wyse 2001b), as well as NGC 1275 itself.

We defined early-type LMCGs (see §1 and Paper III) as objects with low surface brightnesses, low light concentra-

tions, and exponential surface brightness profiles. We furthermore used the constraint that these early-type LMCGs are symmetric objects with no obvious signs of distortions or sub-structure. Our good resolution ($0.7''$) images allow us to make these determinations for even small, faint objects. Note that we only consider objects with sizes $> 1''$ from which we can make these morphological estimates. The summary of these criteria for early-type LMCG classification is the following:

- (i). Total (B-R) color values < 2 . Galaxies redder than this are almost always in the background, although Mobasher et al. (2001) find confirmed faint members of the Coma cluster with colors (B-R) > 2 .
- (ii). Symmetric, round or elliptical shapes, without evidence for internal structures that might be due to star-formation, spiral structures, or other internal features. Background galaxies are often morphologically disturbed and can be identified in high resolution images (e.g., Conselice 2001).
- (iii). A central surface brightness fainter than $\mu_B = 24.0$ mag arcsec $^{-2}$ and a non-centrally concentrated light profile that is close to exponential. These are properties of nearby dwarf ellipticals and can be used for distinguishing dEs from giant ellipticals and background systems. There is some limited overlap in luminosity between the giant ellipticals and the LMCGs.

Any objects that do not meet this criteria, and were not previously identified as stars, are considered background objects. These morphological classifications are the basis for our decisions concerning cluster membership, and for defining different galaxy populations. We did not use the surface-brightness magnitude relationship to define which objects are in the cluster. The good fit between these two parameters is however a check on the reliability of our method for picking out real cluster members (see §3). The final tally is: 160 LMCGs, 28 giant galaxies and 716 background systems.

3. BACKGROUND GALAXIES

The misidentification of background galaxies as true cluster members is a serious problem when trying to study the faintest members of a cluster. Popular techniques to avoid this include subtracting background fields from number counts, although this method possibly under-subtracts the number of background galaxies (Valotto, Moore & Lambas 2001). Another method, used with some success by Secker et al. (1997), rejects galaxies redder than the reddest giant elliptical, and corrects statistically measured properties by using control fields. Other methods utilize morphological information to determine cluster membership (e.g., Binggeli et al. 1985; Ferguson & Sandage 1990). The morphological method is more reliable than one might think a priori; most ($> 90\%$) of objects identified as cluster members using this technique were later confirmed as members from velocity measurements (e.g., Binggeli, Popescu & Tammann 1993; Drinkwater et al. 2000). By far the most reliable method is to base cluster membership on measured radial velocities (e.g., Drinkwater et al. 2001). There are, however, no clusters where redshifts are known for all galaxies with magnitudes in the range of those in the present study. The only clusters where radial velocities of the faintest galaxies (with $M_B > -16$) have been ob-

tained are the nearby Virgo and Fornax clusters (Paper I; Drinkwater et al. 2001).

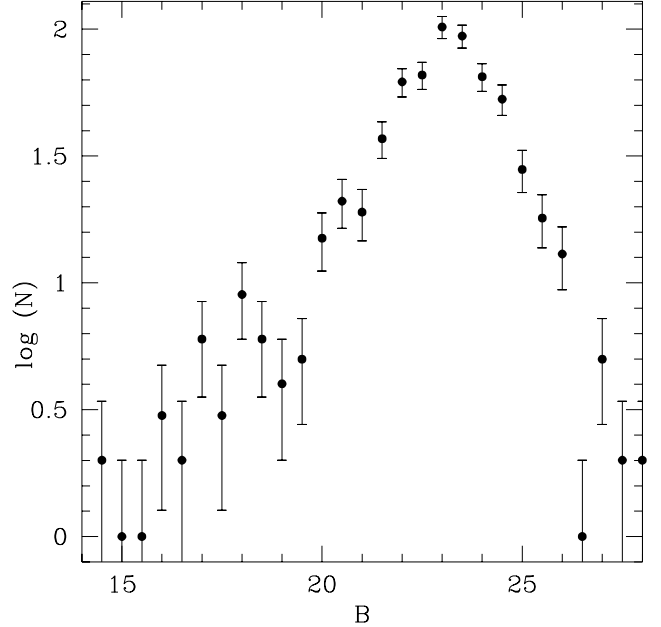


FIG. 4.— Basic luminosity function of all galaxies detected by FOCAS with sizes $R_p > 1''$ in our Perseus survey field in the B band.

Background field galaxies can often be identified by their sub-structures arising from spiral arms or other irregularities produced by star-formation or mergers, which are both common at high redshift (Conselice 2001). From a comparison of images of the Hubble Deep Field taken with the WIYN telescope with the original HST data, Conselice & Gallagher (1999) determined that images such as the ones used in the present study (S2kB camera in good seeing) allow the internal structures of moderate redshift galaxies out to $z \sim 0.5$ to be detected and resolved. The problem with distinguishing background galaxies from faint cluster members is that higher- z galaxies are not only small, but they also have a low surface brightness, due to cosmological dimming, and so can mimic cluster dwarfs. Since most high- z galaxies detectable with WIYN are intrinsically of high surface brightness and have distorted structures, we are able to statistically separate them from cluster LMCGs; we find only two cases of galaxies that might marginally be classified as early-type LMCGs in a WIYN image of the Hubble Deep Field, revealing a very low contamination rate.

To determine if we could morphologically distinguish galaxy populations at intermediate redshifts, we simulated R-band images based on nearby galaxies from Frei et al. (1996) redshifted out to $z \sim 0.5$. Spiral structures were easily visible, although the elliptical galaxies proved to be much harder to distinguish from LMCGs. Ellipticals are however rarely seen in the field or at high- z outside of clusters, and there is no evidence, prior to this paper, for any clusters behind the central region of Perseus. We also set a minimum size limit in FOCAS for detections of candidate Perseus cluster members, of $1''$ (or ~ 300 pc at the distance of the Perseus cluster); most galaxies smaller than this are probably in the background. We conclude it

is likely that actual cluster members can be distinguished from background objects through identifying substructure, although there will inevitably be some misidentifications.

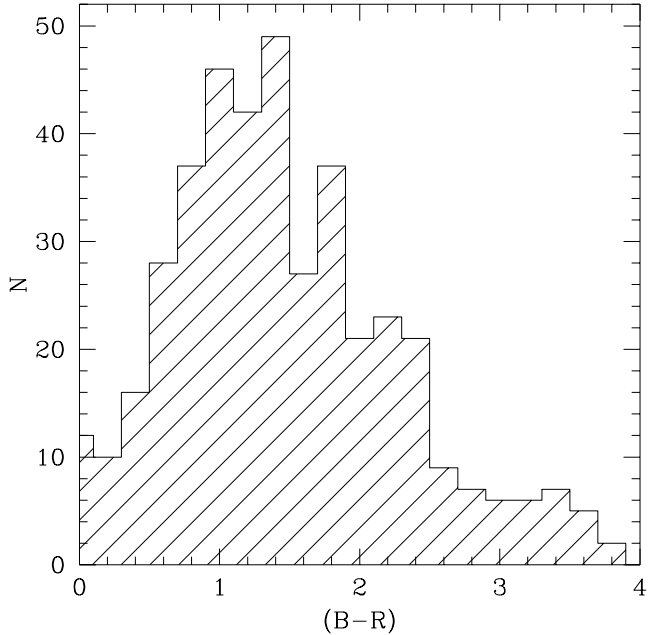


FIG. 5.— Histogram of (B-R) colors of morphologically selected background galaxies seen towards the Perseus cluster center.

Figure 5 shows the resulting color distribution of galaxies in our images that we have classified as being background objects, based on their morphologies. This diagram illustrates a potential problem with using color selection techniques to remove background objects, since the typical range of (B-R) color used to assign cluster membership is $0.9 < (B-R) < 1.8$ (e.g., Secker et al. 1997) and as seen in Figure 5, many galaxies with colors in this range have morphologies consistent with their being background objects. A large fraction of these galaxies have extremely low S/N ratios in the U band, which is another indication that they are background objects since high- z galaxies are usually very faint at shorter observed wavelengths (e.g., Steidel & Hamilton 1992). However, some misidentifications are unfortunately inevitable. This color based rejection technique we and others (e.g., Secker et al. 1997) use will also remove populations of faint cluster galaxies with unusual stellar populations that may exist (e.g., Drinkwater et al. 2001). From other rich clusters, such as Virgo, we know that the faint end of the luminosity function is dominated by structurally smooth early-type LMCGs (Binggeli et al. 1985). As such, our sample contains a *lower* limit to the number of faint galaxies that might exist in the central region of Perseus as any irregular appearing objects will be thrown out as being in the background.

Another indication that we are rejecting mostly true background galaxies comes from the surface brightness-magnitude diagram for objects chosen as cluster and background members (Figure 6). Figure 6 plots the absolute magnitude for cluster members, M_B vs the central surface brightness, μ_B . While nearly all the cluster members fall along a well defined correlation of surface brightness with

magnitude (§4.2), there is a large spread in position of these background objects on the same diagram with apparent magnitude plotted vs. surface brightness (Figure 6b). The dashed curve in Figure 6b shows where elliptical galaxies would be on this diagram if they were at redshifts higher than that of the Perseus cluster. The clump of objects in the upper right of Figure 6b is possibly a background cluster of galaxies at $z \sim 0.55$ (see §4.2 for further discussion). Further proof of the success of this method for identifying background galaxies will require a redshift survey to determine how accurate our estimates are. Another check would be to see if the galaxies we pick out as background systems are distributed in projected space as would be expected in the general background field. If misidentified cluster members were in this sample then we would see a clustering of galaxies towards the center of the cluster. While we do not have the area to fully test this, the background systems do not appear to cluster towards the center of Perseus.

4. ANALYSIS

4.1. The Color-Magnitude Relation

One of the most remarkable properties of cluster galaxies is the presence of a well-defined color-magnitude relationship among the non-dwarf early-type galaxies. This sequence is now well characterized and has been observed in several other nearby clusters, including Coma (e.g., Secker et al. 1997) and Virgo (e.g. Bower, Lucey & Ellis 1992). The color-magnitude relationship in clusters was first discussed in detail by Sandage (1972) and Visvanathan and Sandage (1977) for Coma and Virgo. It is likely a universal relationship that varies little between different nearby clusters (Bower et al. 1992). The color-magnitude relation is also seen in high redshift clusters, with a shift consistent with passive evolution between then and now (Stanford, Eisenhardt & Dickinson 1998). This is usually interpreted as a metallicity effect (e.g., Larson 1974), where more massive galaxies are able to hold on to metals produced in stellar nucleosynthesis and self-enrich through successive generations of stars (cf. Worthey 1994). The lower mass, and hence likely fainter, ellipticals have lower escape speeds and suffer enhanced loss of metal-rich supernova ejecta (e.g., Dekel & Silk 1986). This idea is further suggested by the tight correlation between the strength of the Mg_2 absorption line index and the internal velocity dispersions of early-type galaxies (e.g., Bender, Burstein & Faber 1993).

We investigated this relationship in the Perseus cluster with our UBR photometry down to our completeness limit. We used the $(B-R)_0$ color index, which is a powerful physical diagnostic sensitive to metallicity in old stellar populations such as globular clusters (e.g., Harris 1996). The general color-magnitude trend is confirmed for galaxies in the Perseus cluster with $M_B < -16$ (solid line in Figure 7; note that the colors are the mean within R_p). A least squares fit gives that the relationship between magnitude and color is:

$$(B-R)_0 = (-0.055 \pm 0.009)M_B + (0.456 \pm 0.16), \quad (5)$$

for objects with $M_B < -16$. The relationship between color and apparent magnitude found by Secker et al. (1997) for galaxies in the Coma cluster is: $(B-R)_0 = (-0.056 \pm 0.002)B_0 + (2.41 \pm 0.04)$.

Converting this into an absolute magnitude B-band relation gives

$$(B - R)_0 = (-0.056)M_B + 0.452. \quad (6)$$

Thus, within the errors, the two clusters have identical color-magnitude sequences for the brighter galaxies. The only bright galaxy in the central Perseus cluster region we study that does not fit along the color-magnitude relationship is NGC 1275, a bizarre bright and blue galaxy with recent star-formation that is likely undergoing rapid evolution (Conselice et al. 2001b). It is also the only galaxy over-exposed in both the mini-mosaic and S2kB images and thus does not appear on Figure 7.

As can be seen in Figure 7, there is a large scatter in the color-magnitude relationship at $M_B > -16$. The rms scatter from the color-magnitude relation fiducial sequence, calculated only from galaxies within 1 magnitude of the fiducial to minimize possible contamination from misidentified non-members, is plotted as a function of magnitude in Figure 8. The scatter is very small at $M_B < -16$, $\sim \sigma = 0.07$, but rises to $\sigma = 0.54$ at $M_B = -13$. Out to $M_B = -13$, the scatter can be characterized as

$$\sigma = (0.009 \pm 0.003) \times 10^\gamma, \quad (7)$$

where $\gamma = (M_B + 23.44 \pm 0.89) / (6.81 \pm 0.68)$. This scatter essentially remains unchanged between $M_B = -13$ and $M_B = -11$, potentially the result of the color criteria for membership selection, $(B - R)_0 < 2$, which can remove real cluster members that are very red, decreasing the observed scatter at fainter magnitudes.

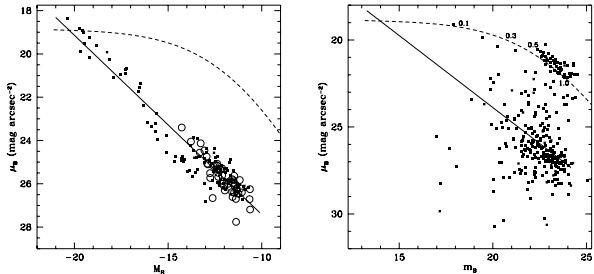


FIG. 6.— Absolute magnitude M_B versus the central ($2''$) surface brightness μ_B for (a) LMCs and ellipticals chosen to be in the cluster. Panel (b) shows the corresponding magnitude-surface brightness plot for objects likely in the background, but plotted against apparent magnitude m_B . The solid small squares in (a) are the 139 objects that are within 2σ of the color-magnitude relationship, including the giant ellipticals (see text). The open circles are the 49 objects redder than 2σ of the color-magnitude relationship. The dashed line shows where a $M_B = -20$ galaxy would be seen on this diagram if it were at redshifts from 0 to 1, with $z = 0.1, 0.3, 0.5$ and 1 labeled on panel (b). The clustering of points at $m_B \sim 23$ and $\mu_B \sim 21$ is possibly a background cluster at $z \sim 0.55$.

A similar large amplitude scatter was observed at these faint magnitudes by Secker et al. (1997), who used a different approach to remove background galaxies. Could this scatter be produced solely from foreground or background misidentified as cluster galaxies? It is unlikely that many of the blue objects in this scatter could be stars, or background/foreground galaxies. Galaxies at higher redshifts undergoing star-formation are not as blue as these objects due to large k-corrections. Since these objects are clearly

resolved they cannot be stars, and they are unlikely to be foreground field galaxies, since very few field dwarfs seem to exist. These objects are also not in any particular part of our fields, such as near large galaxies, as would be expected for globular clusters. Several other groups have recently found a population of red low-luminosity galaxies in, for example, the Fornax (Rakos et al. 2001) and Coma clusters (Adami et al. 2000; Mobasher et al. 2001). However, the red objects have a higher chance of being background objects, and spectroscopy is required to confirm their cluster membership. In Paper III we discuss in detail the likely physical reasons for this scatter, and argue more firmly for its existence.

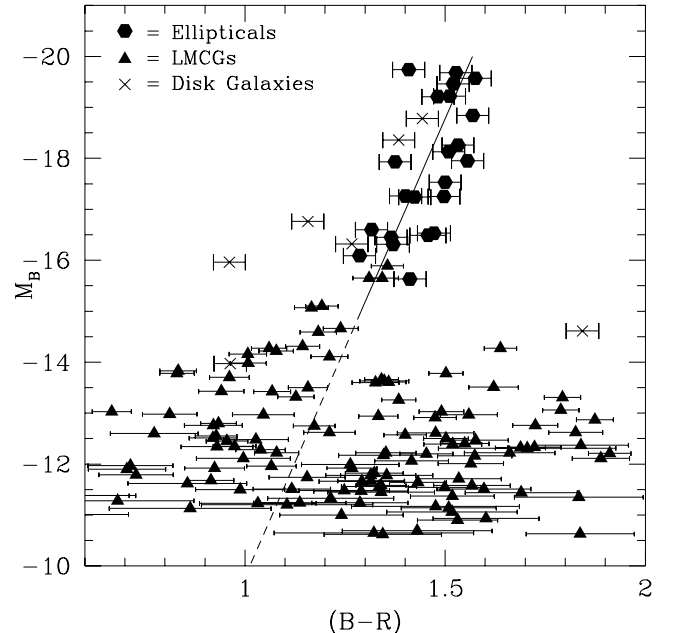


FIG. 7.— Color magnitude diagram of all galaxies identified as candidate cluster members. The solid line shows the proper fit from eq. (5) to the giant ellipticals, and the extension of this correlation to fainter magnitudes is shown as a dashed line.

A (B-R) vs. (U-B) diagram for those galaxies with UBR photometry is shown in Figure 9. Plotted on this diagram are the predictions for single-age, old populations with metallicities between $[\text{Fe}/\text{H}] = 0.5$ to -2. The solid line is a 18 Gyr isochrone, the dashed line is a 12 Gyr one, and the dot-dashed line is a 5 Gyr isochrone. These are based on the stellar synthesis models of Worthey (1994). In these models we use a standard Salpeter IMF slope of 2.35, with a mass range of $0.1 M_\odot - 100 M_\odot$, allowing only passive evolution after an initial single burst of star-formation, and adopt a single global metallicity. This diagram is broadly consistent with the interpretations derived from the color-magnitude relation. The ellipticals are located in a very small locus about $[(\text{U-B}), (\text{B-R})] = [0.5, 1.6]$ while the fainter galaxies with $M_B > -16$ are generally bluer in (B-R) and (U-B) than are the brighter galaxies. For the most part the colors of all galaxies in the central regions of the Perseus cluster are consistent with containing old ($>$ few Gyrs) stellar populations, whose color differences are possibly the result of variations in metallicities (Paper III). The lack of a correlation between color and M_B for lower stellar mass cluster members in

combination with colors typical of older, moderate to high metallicity stellar populations suggests that these objects are more metal-rich and hence could have been, or are, more massive than their luminosity indicates.

4.2. Surface-Brightness Distributions

In this section we investigate trends in the surface brightnesses of Perseus galaxies. When comparing to other studies it must however be remembered that the method we use to define magnitudes differs from previous studies. This, however, does not appear to be important for the photometry, suggesting that the R_p radius is a stable choice for measuring proper magnitudes.

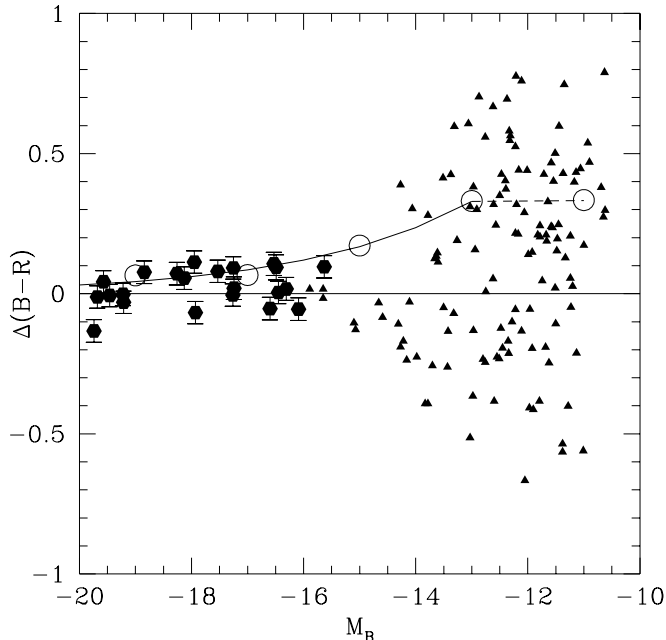


FIG. 8.— Scatter from the color-magnitude relation as a function of absolute magnitude M_B . The open circles are the scatter values at each magnitude range, while the solid line is a fit to these points (see text). Symbols are the same as in Figure 7.

The brightest elliptical galaxies in the S2kB images are over exposed. As such, we use the photometry from the shallower Mini-Mosaic images to complement the fainter elliptical and LMCG photometry from the S2kB detector. Figure 6a shows the relationship between surface brightness, μ_B , as a function of M_B for objects chosen as cluster members. The surface brightness is measured with a central aperture of $2''$. This figure demonstrates the well-known fact (e.g., Binggeli & Cameron 1993) that fainter LMCGs have lower surface brightnesses. The remarkable feature of this diagram is the relatively tight correlation between absolute magnitude and central surface brightness over an 8 magnitude span in brightness. By fitting this relationship by a least square regression, we obtain

$$\mu_B = (0.828 \pm 0.022)M_B + (35.7 \pm 0.3) \quad (8)$$

with a scatter of $\sigma = 0.42 \text{ mag arcsec}^{-2}$ at the bright end, and $\sigma = 0.63 \text{ mag arcsec}^{-2}$ for the faint galaxies. Binggeli & Cameron (1991) find that for the Virgo cluster dwarf ellipticals the relationship $\mu_B = 0.75M_B + 35.3$ holds, again with the dispersion slowly increasing towards the fainter objects.

However, as opposed to Kormendy (1977) and others, we do not generally find that the fainter ellipticals have higher surface brightnesses than the brighter Es. Either the Kormendy (1977) relationship is not strong in the central region of the Perseus cluster, or as based on our luminosity function, we do not have enough bright ellipticals in our sample to see this properly. In particular, we do not have examples of systems which are luminous and have low central surface brightnesses (see e.g., Sandage & Lubin 2001). The Kormendy relationship has previously been found to be weakly present in early type cluster members, other than the most luminous giant ellipticals (Capaccioli & Caon 1991). This result is consistent with observations revealing high surface brightness, ‘cuspy’ centers in moderate luminosity ellipticals and lower brightness cores in the most luminous objects (Faber et al. 1997). We find the same correlation between surface brightness and magnitude for the early-type LMCGs, as for the giants, when we plot the mean surface brightness within R_p , but the LMCGs have a much larger scatter from the fit between surface brightness and magnitude.

The 49 galaxies which are $> 2\sigma$ redder than the relationship in eq. (5), which is plotted in Figure 7, are distinguished by open circles in Figure 6. Perhaps surprisingly, most of these red objects fall along the fitted line in Figure 6. The faint objects that do not fit as well along this surface-brightness/magnitude relationship are the bluer objects (small solid squares), with colors $< 2\sigma$ from the color-magnitude relationship, which are less likely than the redder ones to be in the background. This provides another indication that the faint red objects are actual cluster members, and not background galaxies. If the red objects were ellipticals in, for example, a background cluster, then the total apparent magnitude of the galaxy would be very different than if it were near, but the central surface brightness should stay relatively constant, short of extreme cosmological dimming. These objects would then be above the fitted relationship (eq. 8). The dashed curve in Figure 6 shows where on this diagram a galaxy with $M_B = -20$, observed at redshifts in the range from $z = 0$ to 1, would lie. Clearly, very few objects we selected as cluster members (Figure 6a) fall anywhere near this locus.

Furthermore, Figure 6b shows the surface brightness-magnitude relationship for objects chosen by our criteria to be in the background. Besides the obvious fact that the scatter about the fit from Figure 6a (the solid line) is large, there are objects with surface brightnesses several magnitudes higher than what would be predicted for LMCGs, if they are dwarf-like, based on their magnitudes. Near $m_B = 23$ and $\mu_B = 21$, lying on the dashed curve, there appears to be a cluster of galaxies. If this is a background cluster, its location on this diagram is consistent with $z \sim 0.55$. The brightest galaxies that compose this clump have measured (B-R) colors consistent with this redshift, assuming they are ellipticals (e.g., Fukugita, Shimasaku, & Ichikawa 1995). Objects that compose this clump cluster on the sky, with most of the them in a region of area $\sim 3.5 \text{ arcmin}^2$ centered roughly at (J2000) 03:18:49, +41:33:30. For $H_0 = 70 \text{ km s}^{-1} \text{ Mpc}^{-1}$, $\Omega_M = 1.0$ gives a diameter of 0.59 kpc for this candidate cluster, or 0.72 kpc for $H_0 = 70 \text{ km s}^{-1} \text{ Mpc}^{-1}$, $\Omega_M = 0.3$ and $\Omega_\lambda = 0.7$ both of which are reasonable cluster sizes (e.g.,

Sheldon et al. 2001).

4.3. Structural Parameter Results

Structural parameters provide quantitative information concerning morphologies and properties of galaxies otherwise unobtainable from pure photometry or spectroscopy. In this section we examine the concentration and asymmetry indexes calculated for cluster members, as well as various measurements of radius. Measuring structural parameters of galaxies requires much better resolution and higher signal to noise ratios than those needed to acquire accurate photometry. Because of this, and to limit the effects of any potential contamination from background objects, we make further restrictions in the definition of the sample used to investigate structural parameters. We only examined galaxies with effective (within the half-light radius) surface brightness $\mu_B < 26$ mag arcsec $^{-2}$, and colors of $0.6 < (B-R) < 1.65$. This minimizes contamination from foreground and background objects that are likely to be, in some form, present in the total sample.

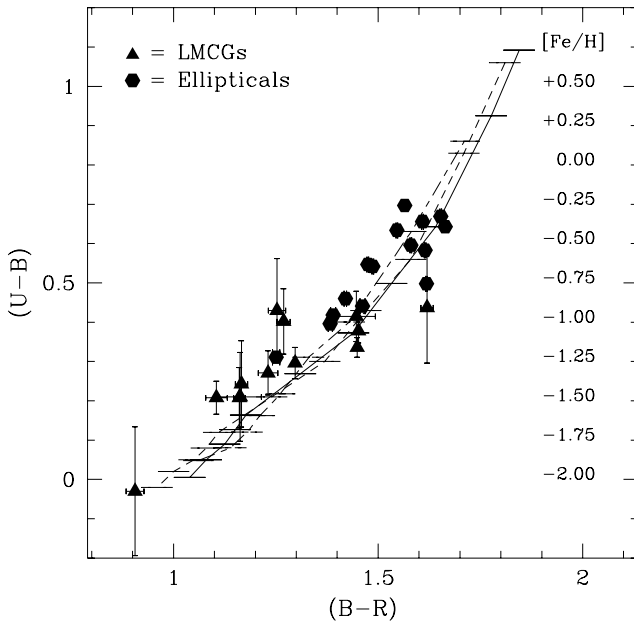


FIG. 9.— UBR color-color diagram of galaxies with U band photometry. The dot-dashed, dashed and solid lines are color isochrones of 5, 12 and 18 Gyr instantaneous burst stellar populations with various metallicities labeled towards the right and denoted as dashed lines on the various isochrones. The brightest elliptical galaxies have metallicities slightly higher than solar.

4.3.1. Asymmetry

The asymmetry structural parameter (see also §2.5) is an effective measurement of the merging, interacting, and star-formation properties of galaxies (Conselice et al. 2000a,b). Briefly, galaxies with low asymmetries and red colors are usually classified as ellipticals, while those with higher asymmetries and bluer colors are disk and irregular galaxies. Galaxies with the highest asymmetries are consistent with interactions or mergers (see Conselice et al. 2000a for a full discussion). After computing the asymmetries of all galaxies, we find the not too surprising result that there is a lack of systems with high asymmetries. In its inner ~ 173 arcmin 2 (~ 0.1 Mpc 3) the Perseus

cluster has only one galaxy consistent with an ongoing major merger, NGC 1275 (Conselice et al. 2001b).

For the most part, cluster giants are found to be consistent with classical ellipticals, with low asymmetries and red colors, as might have been expected. However, we see something different for the LMCGs. Among field galaxies there is a significant trend between asymmetry and $(B-V)_0$ color, a good indicator of recent star-formation (Conselice et al. 2000a). In the Perseus cluster we find no correlation; bluer galaxies, which are LMCGs, are generally symmetric.

Two possible effects are responsible for this lack of an observed correlation between color and asymmetry. The first is that the fainter LMCGs, which are small and blue objects, might not be sufficiently resolved to show any clumpy regions of star-formation (e.g., Gallagher & Hunter 1989). Conselice et al. (2000a) performed simulations on nearby galaxies and determined that a reliable asymmetry can be obtained in galaxies with structures resolved on scales greater than 500 pc. In Perseus, we are resolving scales down to 210 pc. These simulations were however done on large spiral and elliptical galaxies, and they might not be applicable to small early-type LMCGs which may have structures smaller than those found in larger galaxies.

The other possible explanation is that $(B-R)$ is only measuring metallicity, and little to no recent star-formation is present in these systems. This would imply that all of these faint galaxies have been quiescent for several billion years. Use of a color index that is less sensitive to metallicity would then produce a narrower spread in color, and maintain the asymmetry spread.

We conclude from this that most galaxies in the central regions of the Perseus cluster contain old stellar populations, with little to no recent star-formation and $(B-R)$ colors driven primary by metallicity. This is consistent with a lack of H α emission in any galaxy in the central regions of the Perseus cluster, besides the giant elliptical NGC 1275 (Conselice et al. 2001a), and with the UBR diagram (Figure 9) showing the colors of LMCGs match those of old stellar populations with differing metallicities. In Paper III we examine the color maps of the Perseus LMCGs to determine if any stellar population gradients are present.

4.3.2. Radii and Light Concentrations

How do the sizes of Perseus cluster galaxies correlate with other features? Figure 10 shows the relationship between the half-light (or effective) radii, R_e , defined in §2.5, and the total B-band magnitude. In general, brighter galaxies have larger half-light radii; a least-squares fit to all galaxies gives the following correlation:

$$R_e(\text{kpc}) = (-0.1 \pm 0.008) \times M_B - (1.0 \pm 0.1),$$

which is plotted as the solid line in Figure 10. A large amount of the scatter about this relation arises from the disk galaxies. If we consider just the LMCGs then the slope of this correlation becomes steeper. The formal fit restricted to LMCGs is given by:

$$R_{e,\text{LMCG}}(\text{kpc}) = (-0.2 \pm 0.02) \times M_B - (2.3 \pm 0.2),$$

and is shown as a dashed line in Figure 10. These are similar to the relationships found for dwarfs and giants in the Virgo cluster by Binggeli & Cameron (1991).

The concentration index (as defined in §2.5) is measured from the curve of growth of each galaxy. The giant ellipticals are the most concentrated objects, with $C \sim 3$. The LMCGs have a wide range of concentration values, but in general they are the least concentrated objects, demonstrating perhaps a fundamental difference in formation mechanisms.

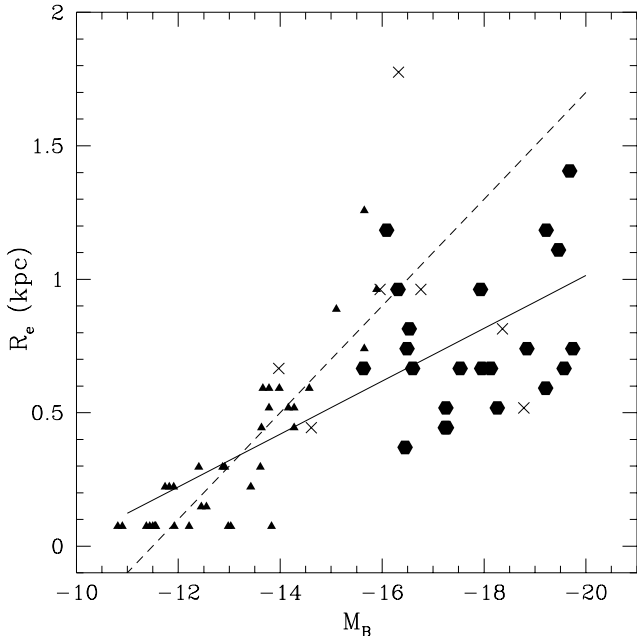


FIG. 10.— Effective radii R_e as a function of absolute magnitude M_B . Symbols are the same as in Figure 7. The solid line is a proper fit to all of the data (see §4.3.2), while the dashed line is a fit to the LMCGs alone.

The low concentration values of the LMCGs are another piece of evidence that these objects are cluster members, and not background galaxies. Galaxies at redshifts $z > 0.1$ typically have intrinsically steep radial profiles if they are ellipticals, or bulge dominated systems. Early-type background galaxies have much higher concentration indexes than those found for a majority of the LMCGs. If background galaxies have pure exponential profiles then they could in principle be misidentified as LMCGs, however these objects are usually too faint and small to be included in the our sample.

4.4. The Perseus Cluster Central Luminosity Function

The number of galaxies per unit magnitude interval is a useful observational constraint to compare galaxy formation scenarios with observational data (e.g., Press & Schechter 1974). A popular method for doing this is to compute luminosity functions (LF) in different environments, especially in clusters. One major reason for fitting luminosity functions is to determine the relative number of low-mass systems in comparison to larger galaxies by measuring the value of the faint-end slope, α which has measured values between ~ -1.0 and -2.3 (e.g., Thompson & Gregory 1993; Biviano et al. 1995; Bernstein et al. 1995; Lopez-Cruz et al. 1997; Secker et al. 1997; Phillips et al. 1998; Trentham 1998; De Propris & Pritchett 1998; Adami et al. 2000; Beijersbergen et al. 2002). The typical way to fit luminosity functions is to model the data with some parameterized fit, such as a power-law or the

Schechter (1976) function which has the form:

$$\phi(L)dL = \phi^*(L/L^*)^\alpha \times \exp(-L/L^*) \frac{dL}{L^*}, \quad (9)$$

where $\phi(L)dL$ is the number of galaxies at luminosity L within the interval dL . The parameters ϕ^* , L^* and α are the normalization, characteristic luminosity and faint-end slope for the luminosity distributions. The Schechter function can be written in terms of magnitudes as,

$$\phi(M) = (0.4 \times \ln 10) \phi^* [10^{0.4(M^* - M)}]^{1+\alpha} \exp[-10^{0.4(M^* - M)}]. \quad (10)$$

Previous to this study, De Propris & Pritchett (1998) obtained a luminosity function for the central regions of the Perseus cluster, finding a faint-end slope $\alpha = -1.56 \pm 0.07$ within the magnitude range $-19.4 < M_I < -13.4$. The Coma cluster is generally observed to have a similar faint end slope of $\alpha = -1.4$ (e.g., Thompson & Gregory 1993; Biviano et al. 1995; Bernstein et al. 1995; Secker et al. 1997; Lopez-Cruz et al. 1997; Beijersbergen et al. 2002).

The WIYN images used here are deeper, by 1 magnitude, than the data used in De Propris & Pritchett (1998), assuming a typical color of $B-I = 1.6$ for the lowest luminosity galaxies. As was shown in §3, we are likely incomplete at magnitudes fainter than $M_B = -10.7$. Figure 11 shows the resulting luminosity function to this limit, after removing all likely background candidates. We fitted the Schechter function and a power law, of the form $dN/dL = L^\alpha$, to these number counts by using a weighted χ^2 maximum-likelihood minimization method. The resulting fit to the number counts is shown in Figure 11 as a solid line. The faint-end slope is computed as $\alpha = -1.44 \pm 0.04$, with M^* fixed to -19 , although note that the value of the slope α is not highly dependent on the choice of M^* . Fitting the luminosity function to a power-law gives a slope of $\alpha = -1.42 \pm 0.03$. These values are slightly flatter than the slope found by De Propris & Pritchett (1998).

This suggests that perhaps in addition to a universal color-magnitude relation for bright cluster galaxies, there is a consistent process at work to produce the same faint luminosity functions in some rich clusters. Differences between galaxies in clusters seem to be limited to an increased dispersion in the color-magnitude relation for the faint galaxies, and an observed variations in the structural and evolutionary properties of the brightest cluster galaxies. It appears that the faintest and very brightest galaxies in clusters are undergoing the most active evolution over the last few Gyrs (Conselice et al. 2001a,b). Paper III will address, among other things, possible scenarios for the formation of these low-mass galaxy systems.

4.5. Properties of Unusual Perseus Galaxies

Our high quality WIYN images allow an unprecedented opportunity to study individual galaxies in the Perseus cluster (cf. Conselice et al. 2001b for NGC 1275). We examine the detailed properties of the low-mass Perseus galaxies in Paper III; there are, however, two interesting examples of unusual galaxies that we briefly discuss here.

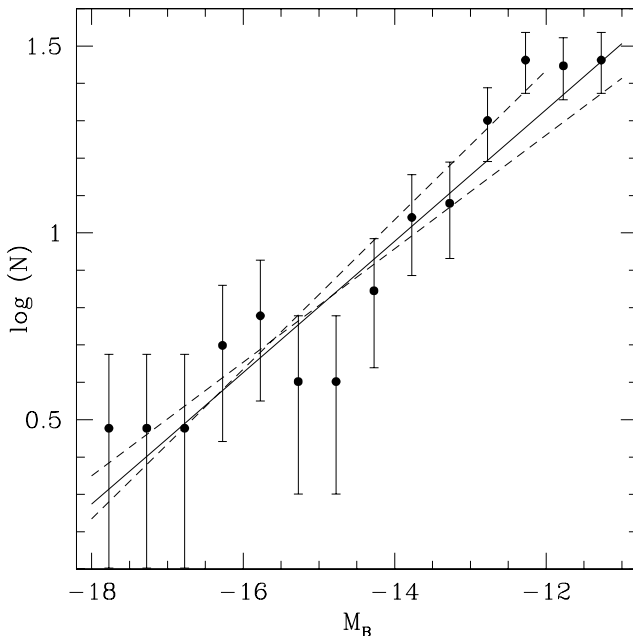


FIG. 11.— The luminosity function for galaxies with $M_B > -18$ in the central region of the Perseus cluster. The solid line is the proper fit, while the dashed lines are 1σ variations on this fit.

After examining the outer isophotes of all ellipticals in the sample, we noticed that one, located at a projected distance of 110 kpc from NGC 1275, shows isophote twists (Figure 12b). Elliptical isophotes are fit to this galaxy by using the Fourier fitting series described in Jedrzejewski (1987). For comparison, Figure 12a shows a normal, typical Perseus elliptical galaxy, its ellipticity profiles (defined as $1-b/a$), and the positional angle of its major axis as a function of distance from its center. The position angle remains roughly constant with radius until $\sim 20''$, when the ellipticity becomes too low to produce an accurate measurement. The change in position angle of the isophotes for the galaxy in Figure 12b indicate either a triaxial shape, or that the galaxy has intrinsic twists that are perhaps remnants of interactions or from disk galaxy mergers that formed the elliptical (Gerhard 1983). This is the only elliptical with this property in the central region of the Perseus cluster. The lack of twists in general is another indication that giant cluster galaxies are a long-established population, since otherwise one might expect structural remnants would remain from recent mergers (e.g., Gerhard 1983). The far right column in Figure 12 shows the coefficients a_4 of the Fourier fits to the isophotal shapes. This component reveals if the isophotes deviate from pure ellipses. All three galaxies shown have an average $a_4 \sim 0$, indicating that the structures are not dominated by boxy or disk-like isophotes.

The galaxy at the bottom of Figure 12 is an unusual object only ~ 35 kpc projected distance from NGC 1275. This galaxy is located at (J2000) 03:19:39.6, +41:31:04 and is called SA0426-002 in Conselice & Gallagher (1999). As can be seen, this galaxy has a butterfly shape, with low surface brightness ‘wings’, with $\mu_B = 27$ mag arcsec^{-2} . The core of the galaxy is also unusual; it is a linear, almost bar-like object, that gets broader with radius. This strange object is perhaps the result of a dynamical interaction with NGC 1275, with the Perseus cluster’s potential or with some other individual galaxy. It could also be an object seen in an unusual projection, such as a disk galaxy with an outer ring that has had its spiral arms removed by tidal effects. Figure 12c shows the surface brightness profile of this galaxy, together with the best-fit Sersic profile of the form

$$I = I_0 \times \exp[-(r/r_0)^{(1/n)}].$$

This best-fit profile, with $n = 1.19 \pm 0.08$, is close to a pure exponential. This galaxy has a rather blue color, $(B-R) = 1.3$, and faint absolute magnitude, $M_B = -16.3$. This is faint enough for this object to be a type of dwarf galaxy. This galaxy deserves further attention, since no galaxy known to the authors has a similar morphological appearance.

5. SUMMARY

In this paper we present quantitative techniques for analyzing deep images of galaxy clusters to investigate galaxy evolution. We illustrate this using new photometric data, obtained with the WIYN 3.5-m telescope, for galaxies with $M_B < -11$ in the central regions of the nearby rich galaxy cluster Abell 416 (Perseus). We demonstrate that with the use of non-biased detection, photometric, and structural analysis techniques, we can reduce background galaxy contamination. Using this selected sample of cluster members, we decipher the demographics of central members of the Perseus cluster. The main observational results are:

(i) There are two separate early-type galaxy ‘populations’ in the central region of Perseus based on photometric scaling relationships – a bright one at $M_B < -16$, and a distinct fainter one at $M_B > -16$ containing early-type low-mass cluster galaxies (LMCGs, defined in §1). There is a considerable scatter among LMCGs from the ‘universal’ color-magnitude relation, extrapolated from a fit to the bright ellipticals, for galaxies with $M_B > -16$. The scatter continues to increase at fainter magnitudes up to $M_B = -13$, a point we discuss further in Paper III of this series.

(ii) The number counts of galaxies in the Perseus central region can be fit by a Schechter function with a faint-end slope $\alpha = -1.44 \pm 0.04$, close to values found in other clusters. The color-magnitude relation is found to have a slope, for galaxies brighter than $M_B = -16$, of $(B-R)/M_B = 0.055 \pm 0.009$, similar to that found for Coma (Secker et al. 1997). We find that surface brightness scales with luminosity for all early-type cluster members. Taken as a group, the photometric properties of Perseus cluster early-type LMCGs are indistinguishable from those of dwarfs in the less rich Virgo and Fornax clusters, or in the richer Coma cluster.

(iii) Aside from the complex NGC 1275 system (Conselice et al. 2001b), we find few unusual galaxies, or galaxies undergoing rapid evolution in the Perseus cluster core. Only two galaxies have evidence for a non-passive evolution during the last few Gyrs. The Perseus cluster center therefore contains galaxies that are mostly relaxed and composed of old stellar populations that were in place several Gyrs ago. These results imply that rich cluster galaxy formation is largely consistent with an early formation and later passive evolution for the most massive galaxies (Springel et al. 2001). There appears to be a possible separate process

for the faint cluster galaxies, as they do not follow the same color-magnitude scaling relationship. Despite this, the similar faint-end luminosity slopes and mean LMCG color-magnitude relations in nearby clusters suggests that whatever process is responsible for creating the faintest galaxies in the center of Perseus is possibly occurring in other clusters. On the other hand it must be kept in mind that Perseus is not a typical rich cluster given its very high galaxy density and its other extreme properties that might make galaxies in its center region unique from other clusters. Similar analyses of galaxy populations covering a wide range in luminosity in other clusters are required to determine this.

We thank the staff of WIYN for their support of these observations and the referee for helpful comments. This research was supported in part by the National Science Foundation (NSF) through grants AST-9803018 to the University of Wisconsin-Madison and AST-9804706 to Johns Hopkins University. CJC acknowledges support from a Grant-In-Aid of Research from Sigma Xi and the National Academy of Sciences (NAS) as well as a Graduate Student Researchers Program (GSRP) Fellowship from NASA and from the Graduate Student program at the Space Telescope Science Institute (STScI). RFGW acknowledges a Visiting Fellowship from the UK PPARC.

REFERENCES

Abraham, R.G., Valdes, F., Yee, H.K.C., & van den Bergh, S. 1994, AJ, 432, 75

Adami, C., Ulmer, M.P., Durret, F., Nichol, R.C., Mazure, A., Holden, B.P., Romer, A.K., & Savine, C. 2000, A&A, 353, 930

Allen, S.W., & Fabian, A.C. 1997, MNRAS, 286, 583

Baum, W., Hammergren, M., Thomsen, B., Groth, E. J., Faber, S. M., Grillmair, C.J., & Ajhar, E.A. 1997, AJ, 113, 1483

Beijersbergen, M., Hoekstra, H., van Dokkum, P.G., & van der Hulst, T. 2002, MNRAS, 329, 385

Bender, R., Burstein, D., & Faber, S.M. 1993, ApJ, 411, 153

Bernstein, G.M., Nichol, R.C., Tyson, J.A., Ulmer, M.P., & Wittman, D. 1995, AJ, 110, 1507

Bershady, M.A., Jangren, A., & Conselice, C.J. 2000, AJ, 119, 264

Binggeli, B., Sandage, A., & Tammann, G.A. 1985, AJ, 90, 1681

Binggeli, B., & Cameron, L.M. 1991, A&A, 252, 27

Binggeli, B., & Cameron, L.M. 1993, A&AS, 98, 297

Binggeli, B., Popescu, C.C., & Tammann, G.A. 1993, A&AS, 98, 275

Biviano, A., Durret, F., Gerbal, D., LeFevre, O., Lobo, C., Mazure, A., & Slezak, E. 1995, A&A, 297, 601

Blanton, M.R., et al. 2001, AJ, 121, 2358

Bower, R.G., Lucey, J., & Ellis, R.S. 1992, MNRAS, 254, 601

Brunzendorf, J., & Meusinger, H. 1999, A&AS, 139, 141

Capaccioli, M., & Caon, N. 1991, MNRAS, 248, 523

Cardelli, J.A., Clayton, G.C., & Mathis, J.S. 1989, ApJ, 345, 245

Colless, M., & Dunn, A.M. 1996, ApJ, 458, 435

Conselice, C.J. 1997, PASP, 109, 1201

Conselice, C.J., & Gallagher, J.S. 1999, AJ, 117, 75

Conselice, C.J., Bershady, M.A., & Jangren, A. 2000a, ApJ, 529, 886

Conselice, C.J., Bershady, M.A., & Gallagher, J.S. 2000b, A&A, 354, 21L

Conselice, C.J., Gallagher, J.S., & Wyse, R.F.G. 2001a, ApJ, 559, 791 (Paper I)

Conselice, C.J., Gallagher, J.S., & Wyse, R.F.G. 2001b, AJ, 122, 2281

Conselice, C.J., Gallagher, J.S., & Wyse, R.F.G. 2002, AJ, in prep (Paper III)

Conselice, C.J. 2001, in "ESO/STScI Workshop on Deep Fields", in press.

Dekel, A., & Silk, J. 1986, ApJ, 303, 39

Dalcanton, J.J. 1998, ApJ, 495, 251

De Propris, R., & Pritchett, C.J. 1998, AJ, 116, 1118

Drinkwater, M.J., et al. 2000, A&A, 355, 900

Drinkwater, M.J., Gregg, M.D., Holman, B.D., & Brown, M.J.I. 2001, MNRAS, 326, 1076

Faber, S.M., et al. 1997, AJ, 114, 1771

Ferguson, H.C., & Sandage, A. 1990, 100, 1

Ferguson, H.C., & Binggeli, B. 1994, A&ARv, 6, 67

Frei, Z., Guhathakurta, P., Gunn, J.E., & Tyson, J.A. 1996, AJ, 111, 174

Fukugita, M., Shimasaku, K., & Ichikawa, T. 1995, PASP, 107, 945

Gallagher, J.S., & Hunter, D.A. 1989, AJ, 98, 806

Gerhard, O.E. 1983, MNRAS, 203, 19

Giradi, M., Escalera, E., Fadda, D., Giuricin, G., Mardirossian, F., & Mezzetti, M. 1997, ApJ, 482, 41

Harris, W.E. 1996, AJ, 112, 1487

Ichikawa, S.-I., Wakamatsu, K.-I., & Okamura, S. 1986, ApJS, 60, 475

Jarvis, J.F., & Tyson, J.A. 1981, AJ, 86, 476

Jedrzejewski, R.I. 1987, MNRAS, 226, 747

Kauffmann, G., & Charlot, S. 1998, MNRAS, 294, 705

Kent, S.M., & Sargent, W.L.W. 1983, AJ, 88, 697

Kent, S.M. 1985, ApJS, 59, 115

Kormendy, J. 1977, ApJ, 218, 333

Kron, R. G. 1995, in "The Deep Universe," Saas-Fee Advanced Course 23, (Springer), 233

Larson, R.B. 1974, MNRAS, 169, 229L

Lopez-Cruz, O., Yee, H.K.C., Brown, J.P., Jones, C., & Forman, W. 1997, ApJ, 475, L97

Mohr, J. J., Fabricant, D. G., & Geller, M. J. 1994, ApJ, 413, 492

Mobasher, B., et al. 2001, ApJS, 137, 279

Mori, M., & Burkert, A. 2000, ApJ, 538, 559

Nulsen, P.E.J., & Fabian, A.C. 1980, MNRAS, 191, 887

Petrosian, V. 1976, ApJ, 209, 1L

Phillips, S., Parker, Q.A., Schwartzenberg, J.M., & Jones, J.B. 1998, ApJ, 493, L59

Poggianti, B.M. 1997, A&AS, 122, 399

Press, W., & Schechter, P. 1974, ApJ, 187, 425

Rakos, K., Schombert, J., Maitzen, H.M., Prugovecki, S., & Odell, A. 2001, AJ, 121, 1974

Sandage, A. 1972, ApJ, 176, 21

Sandage, A., & Perelmuter, J.-M. 1990, ApJ, 350, 481

Sandage, A., & Lubin, L.M. 2001, AJ, 121, 2271

Schechter, P. 1976, ApJ, 203, 297

Schlegel, D.J., Finkbeiner, D.P., Davis, M. 1998, ApJ, 500, 525

Secker, J., Harris, W.E., & Plummer, J.D. 1997, PASP, 109, 1377

Sheldon, E.S., et al. 2001, ApJ, 554, 881

Sijbring, D., & DeBruyn, A. G. 1998, A&A, 331, 901

Slezak, E., Durret, F., & Gerbal, D. 1994, AJ, 108, 1996

Springel, V., White, S.D.M., Tormen, G., & Kauffmann, G. 2001, MNRAS, 328, 726

Stanford, S.A., Eisenhardt, P.R., & Dickinson, M. 1998, ApJ, 492, 461

Steidel, C.C., & Hamilton, D. 1992, AJ, 104, 941

Struble, M.F., & Rood, H.J. 1999, ApJS, 125, 35

Thompson, L.A., & Gregory, S.A. 1993, AJ, 106, 2197

Trentham, N.D. 1998, MNRAS, 294, 193

Ulmer, M.P., et al. 1980, ApJ, 236, 58

Valotto, C.A., Moore, B., & Lambas, D.G. 2001, ApJ, 546, 157

van den Bergh, S. 1998, *Galaxy Morphology and Classification*, Cambridge University Press

Vazdekis, A., Kuntschner, H., Davies, R.L., Arimoto, N., Nakamura, O., & Peletier, R. 2001, ApJ, 551, 127L

Visvanathan, N., & Sandage, A. 1977, ApJ, 216, 214

Worthey, G. 1994, ApJS, 95, 107

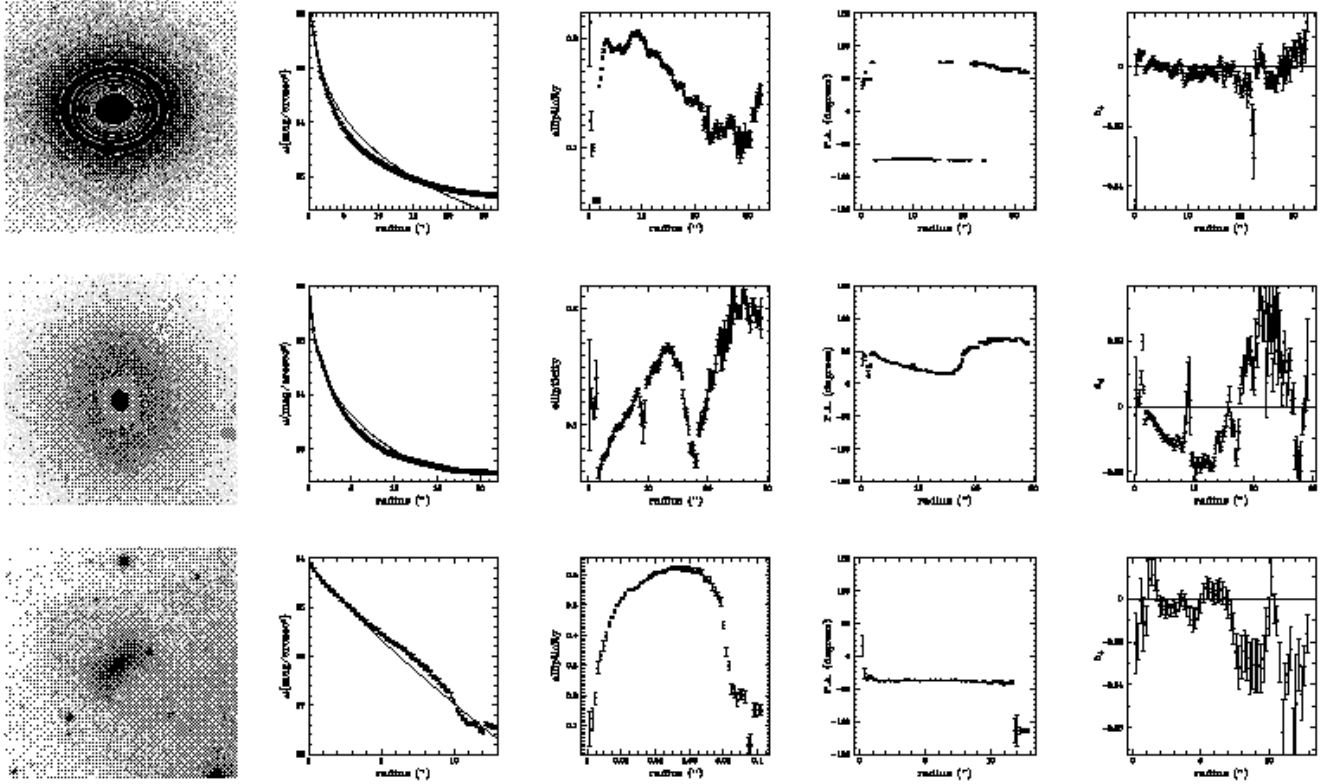


FIG. 12.— Sample of galaxies in the center of Perseus: (a) a normal Perseus elliptical galaxy, (b) an elliptical with twisting isophotes, (c) a symmetric galaxy with a peculiar morphology. The first column shows the image of each galaxy, while the remaining columns are the surface brightness profiles with the best Sersic fit shown, and ellipticity, position angle, and a_4 component as a function of radius.